catalysts

MDPI

Article

Effect of the Colloidal Preparation Method for Supported Preformed Colloidal Au Nanoparticles for the Liquid Phase Oxidation of 1,6-Hexanediol to Adipic Acid

Eleonora Monti [1], Alessia Ventimiglia [1], Carolina Alejandra Garcia Soto [1], Francesca Martelli [1], Elena Rodríguez-Aguado [2], Juan Antonio Cecilia [2], Achraf Sadier [3], Francesca Ospitali [1], Tommaso Tabanelli [1], Stefania Albonetti [1], Fabrizio Cavani [1], Robert Wojcieszak [3,*], and Nikolaos Dimitratos [1,*]

[1] Dipartimento di Chimica Industriale "Toso Montanari", Alma Mater Studiorum Università di Bologna, Viale Risorgimento 4, 40136 Bologna, Italy; eleonora.monti8@unibo.it (E.M.); alessia.ventimiglia3@unibo.it (A.V.); carolina.garcia-soto@lpp.polytechnique.fr (C.A.G.S.); francesca.m.martelli@gmail.com (F.M.); francesca.ospitali@unibo.it (F.O.); tommaso.tabanelli@unibo.it (T.T.); stefania.albonetti@unibo.it (S.A.); fabrizio.cavani@unibo.it (F.C.)

[2] Departamento de Química Inorgánica, Cristalografía y Mineralogía (Unidad Asociada al ICP-CSIC), Facultad de Ciencias, Universidad de Málaga, Campus de Teatinos, 29071 Málaga, Spain; aguadoelena5@gmail.com (E.R.-A.); jacecilia@uma.es (J.A.C.)

[3] University Lille, CNRS, Centrale Lille, Univ. Artois, UMR 8181–UCCS–Unité de Catalyse et Chimie du Solide, F-59000 Lille, France; achraf.sadier@univ-lille.fr

* Correspondence: robert.wojcieszak@univ-lille.fr (R.W.); nikolaos.dimitratos@unibo.it (N.D.)

Citation: Monti, E.; Ventimiglia, A.; Garcia Soto, C.A.; Martelli, F.; Rodríguez-Aguado, E.; Cecilia, J.A.; Sadier, A.; Ospitali, F.; Tabanelli, T.; Albonetti, S.; et al. Effect of the Colloidal Preparation Method for Supported Preformed Colloidal Au Nanoparticles for the Liquid Phase Oxidation of 1,6-hexanediol to Adipic Acid. *Catalysts* **2022**, *12*, 196. https://doi.org/10.3390/catal12020196

Academic Editor: Werner Oberhauser

Received: 17 January 2022
Accepted: 01 February 2022
Published: 4 February 2022

Abstract: Supported on activated carbon gold colloidal nanoparticles have been prepared in the presence of the stabilizing polymer PVA and PVP (polyvinylalcohol, polyvinylpyrrolidone). The effect of the polymer to the Au weight ratio was investigated, for synthesizing gold nanoparticles with different particle size and particle size distribution. By varying the polymer/Au *wt*/*wt* ratio, gold nanoparticles with mean diameters from 3 to 8 nm were synthesized. The synthesized Au catalysts were studied in the liquid phase oxidation of 1,6-hexanediol (HDO) to adipic acid under base and base-free conditions. A range of experimental parameters were varied for the optimization of reaction conditions and the most promising Au catalysts were further evaluated in terms of catalytic performance. We demonstrated that the influence of choice of polymer, tuning the polymer to Au weight ratio, HDO to Au molar ratio, and use of basic conditions have an important influence in terms of catalytic activity and selectivity to adipic acid. The highest yield to adipic acid was obtained using Au-PVA catalysts (40% at 110 °C under base free conditions), however, at low HDO to Au molar ratio and lower carbon balance (70–80%). On the contrary, at higher HDO to Au molar ratio, and under basic conditions, the yield was in the range of 18–20% with a significant improvement in terms of carbon balance (88–100%).

Keywords: supported Au colloidal nanoparticles; effect of stabilizer; production of adipic acid

1. Introduction

1,6-hexanediol (HDO) is an emerging building-block chemical, which may be generated from biomass and transform to adipic acid (AA). AA is one of the key aliphatic dicarboxylic acids widely used in chemical industries as a starting material in the polyamide (nylon-6,6) synthesis. It is also generally used for the production of aliphatic esters, lubricants, and many other applications [1,2]. Its world production reached 3000 kt in 2020 and it is predicted to increase by 2% each year [3]. AA used in chemical industry is generally produced in a two-step oxidation process. The cyclohexane is firstly oxidized to a mixture of cyclohexanone/cyclohexanol (ketone-alcohol, KA oil) and then the oxidation of KA oil to AA. The first step is carried out using air as oxidant and the second

using an excess of HNO_3. From the environmental point of view, this method is seriously harmful due to the production of nitrous oxide (N_2O) which is major responsible for the ozone depletion [4]. For these reasons, the bio-based synthesis of AA has seriously become an alternative candidate to the petrol-based process [5,6]. 99% yield of AA was obtained by the hydrogenolysis of C–O bond in tetrahydrofuran-2,5-dicarboxylic acid (hydrogenated 2,5-furandicarboxylic acid, FDCA) [7]. AA could be also produced from glucose via two-step process [8,9]. However, the low yield of glucaric acid produced in the first step is still a serious drawback. Recently, another bio-based way has been taken attention for the production of AA either by oxidative cleavage of trans-1,2-cyclohexanediol or by the oxidation of HDO. In the presence of 1 wt % Au/C catalyst, 97% yield of sodium adipate was achieved, when the reaction was done for 4 h under 10 bar of oxygen at 70 °C using 1 M NaOH [10]. Au-based catalysts showed advantages over Pt- and Pd-based materials in terms of activity, stability, and selectivity during the aqueous phase oxidation processes. The stability of Au-based catalysts in water and its resistance against molecular oxygen accord the superiority over Pt-and Pd-based materials [11,12].

Moreover, a number of scientific studies revealed that the catalytic activity and stability were notably improved in the presence of Au-Pd of Au-Pt alloy [12–17]. At 140–160 °C and under 6 bar of oxygen and 34 bar of nitrogen, the oxidation reaction of 0.1 M HDO produced AA with 99% yield after 2 h in the presence of 2 wt % Au– 0.1 wt % Pt and 2 wt % Au–0.1 wt % Pd bimetallic catalysts [18]. Another example of bimetallic gold based catalyst (Au-Pt/ZrO_2, n_{Au}/n_{Pt} = 1) has been reported in the aqueous phase oxidation of 0.2 M HDO, but for longer reaction time (48 h). Under 40 bar of air and at 70 °C, 96% yield of AA was reached with full conversion. [19,20]. AA was produced from HDO through sequential oxidation as shown in Scheme 1. HDO is firstly oxidized from one side forming 6-hydroxyhexanal (HH) as an intermediate. It could be then isomerized to oxepan-2-ol. This intermediate is subsequently oxidized to 6-hydroxyhexanoic acid (HHA) and isomerized to ε-caprolactone. AA is finally obtained by subsequent oxidation of HA via 6-oxohexanoic acid (OH).

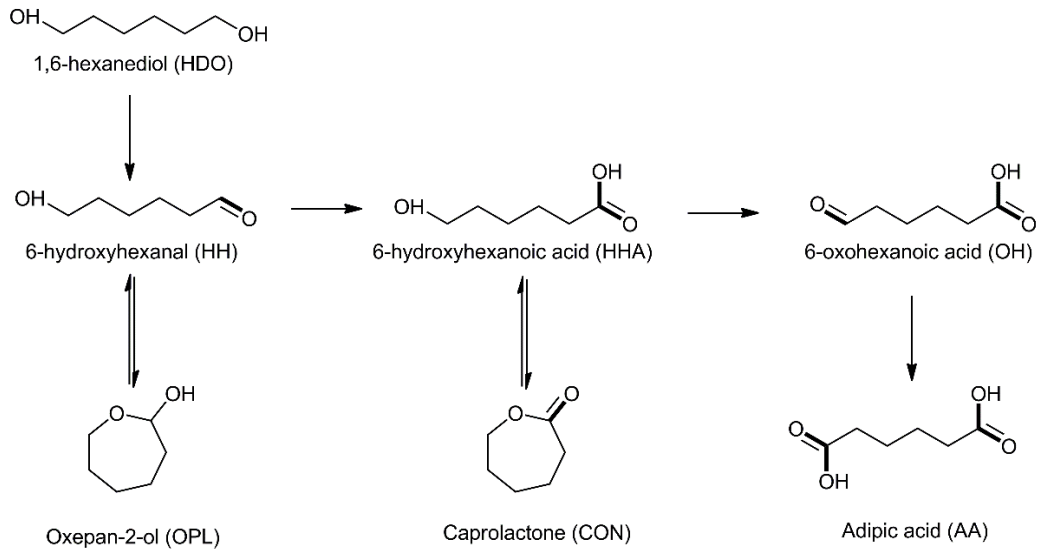

Scheme 1. Oxidation of 1,6-hexanediol to adipic acid.

The objective of this paper is to study the influence of the colloidal preparation method for supported preformed colloidal Au nanoparticles for the liquid phase oxidation of 1,6-hexanediol to adipic acid. Especially, the influence and the role of the stabilizer was studied in terms of controlling the morphological properties of the preformed supported nanoparticles and influencing catalytic activity, stability, and selectivity to the desired product. Two different stabilizers were used: poly(vinyl alcohol) (PVA) and poly(vinyl pyrrolidone) (PVP). The effect of the stabilizer to Au weight ratio

was studied as it is known that has influence in: (i) controlling particle size of the metal and (ii) affecting dispersion of the preformed metal nanoparticles on the support and finally influencing catalytic activity due to the amount of the polymer presented on the surface of the catalyst [21–30]. Moreover, reaction parameters such as stirring rate, time, temperature, substrate to NaOH ratio were studied. The catalysts were characterized by standard techniques before and after catalytic tests.

2. **Results and Discussion**

2.1. Characterization of the Catalysts

The synthesized Au colloidal nanoparticles with PVA and PVP as the chosen stabilizers and different stabilizer/Au weight ratio were analyzed by UV–visible spectroscopy. UV–visible spectroscopy of Au colloidal nanoparticles was used to monitor the intensity and position of the plasmon resonance band of gold [31,32].

Wolfgang Haiss et al. has reported that the dimension of the gold nanoparticles changes the position of the surface plasmon peak [33]. For the Au-PVA colloidal nanoparticles (Figure S1), the UV–vis spectra showed that with increasing the amount of PVA from a polymer:Au weight ratio of 0 to 2.4, the plasmonic peak became flattered and shifted to a lower wavelength. In particular, Au sol without the presence of stabilizer (PVA/Au = 0 w/w) showed the plasmonic peak at 515 nm and Au with PVA to Au weight ratio of 2.4 (PVA/Au = 2.4 w/w) at 503 nm. This plasmon resonance peak is characteristic for gold nanoparticles with particle sizes below 10 nm [13,34]. These results confirm that a higher amount of PVA facilitates the formation of smaller gold nanoparticles in the colloidal solution in agreement with previous reports [21].

In the case of the Au-PVP colloidal nanoparticles stabilized by PVP (Figure S2), the variation of the PVP amount gave a surface plasmon resonance peak, which varied from 498 nm to 500 nm, therefore the surface resonance peaks indicated the presence of small Au nanoparticles when PVP is used in agreement with literature [24,35–37].

XRD analysis was carried out to calculate the average Au crystallite size for the Au/AC samples, estimated from the line-width of the Au (111) diffraction peak at 2θ = 38.2°. When PVA was the chosen stabilizer, in the absence of stabilizer, larger Au nanoparticles were formed, whereas with the progressive increase of the polymer amount a decrease of the mean Au crystallite size was observed (Figure S3, Table S1). In the case of PVP as the chosen stabilizer, larger Au nanoparticles were formed and an increase of PVP/Au weight ratio above 0.6 led to an increase of the mean gold crystallite size (Table S2).

TEM analysis was performed for the Au/AC catalysts to determine the mean gold particle size and gold particle size distribution. Representative STEM-HAADF images for selected Au/AC_PVA catalysts are shown in Figure 1 and TEM images and histograms are shown in Figures S4 and S5 for the Au/AC catalysts using PVA and PVP as stabilizers. The mean Au particle size (Table 1) was reduced by increase of the PVA amount in agreement with the XRD data. The influence of PVA was evident by comparing the TEM images of Au/AC (PVA/Au = 0 *w*/*w*) with Au/AC (PVA/Au = 2.4 *w*/*w*). In the absence of PVA, the presence of larger and agglomerated Au nanoparticles was evident with poor dispersion of the Au nanoparticles on the surface of the support and mean Au particle size of 7.9 nm. On the contrary, by increasing the PVA amount, a decrease of the mean gold particle size followed by a narrower particle size distribution was observed. For example, Au/AC (PVA/Au = 2.4 w/w) catalyst showed a narrow particle size distribution and mean gold particle size of 2.4 nm, with good dispersion of the Au nanoparticles. In the case of Au/AC catalysts with PVP as the chosen stabilizer, the trend was not the same as in the case of PVA. In the presence of PVP, and when the PVP/Au weight ratio was in the range of 0.3–0.6 the mean gold particle size was around 5.5 nm. At higher PVP/Au weight ratio an increase of the mean Au particle size was observed, indicating the

significant role of the nature of the stabilizer to influence the dispersion of the nanoparticles onto the support.

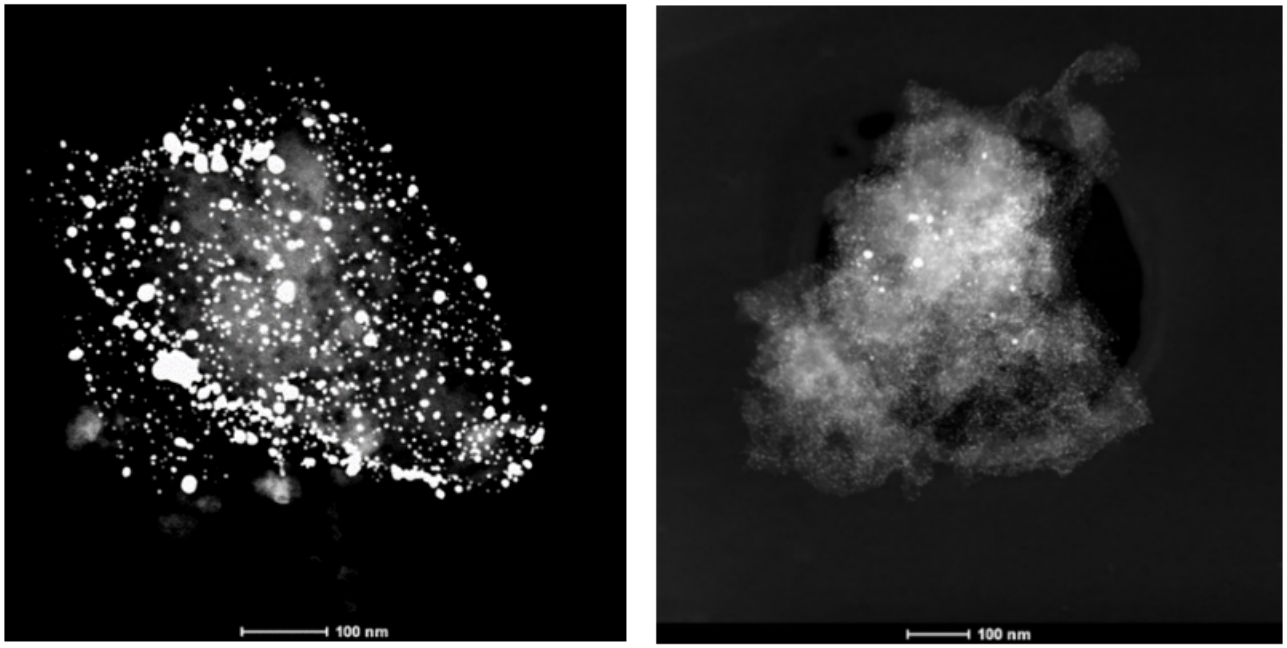

(**a**) (**b**)

Figure 1. Representative STEM-HAADF images of (**a**) Au/AC (PVA/Au = 0 *w*/*w*) and (**b**) Au/AC (PVA/Au = 2.4 *w*/*w*).

Table 1. Mean particle size for supported Au nanoparticles using PVA and PVP with different polymer to Au weight ratio as determined by TEM analysis.

Samples	Stabilizing Polymer	Polymer:Au Weight Ratio	Mean Particle Size of Au (nm)
Au/AC_0	None	0	7.9 ± 6.3
Au/AC_PVA_0.3	PVA	0.3	4.3 ± 3.6
Au/AC_PVA_0.6		0.6	2.7± 1.6
Au/AC_PVA_1.2		1.2	2.6± 2.1
Au/AC_PVA_2.4		2.4	2.4± 1.2
Au/AC_PVP_0.3	PVP	0.3	5.5± 3.6
Au/AC_PVP_0.65		0.65	5.6 ± 3.9
Au/AC_PVP_1.2		1.2	7.4± 4.7
Au/AC_PVP_2.4		2.4	8.4 ± 4.9

XPS analysis of the Au/AC catalysts was performed to investigate the oxidation state of the Au and the surface atomic composition, focusing on the Au/C surface atomic ratio. In the Au 4f region the presence of Au species is illustrated by two peaks, corresponding to Au $4f_{7/2}$ and Au $4f_{5/2}$ transitions. We refer for comparison the values of binding energies to the Au $4f_{7/2}$ peak. The results are presented in Figures S6 and S7 and Table 2. The Au $4f_{7/2}$ binding energies were in the range of 84.0–84.1 eV, this range is consistent with the presence of Au in a metallic state (Au^0) [38–40]. Increasing the PVA/Au weight ratio from 0 to 0.3 an initial increase of the Au/C surface atomic ratio was observed from 0.028 to 0.039, whereas a further increase of the PVA/Au weight ratio from 0.3 to 2.4 led to a decrease of the Au/C surface atomic ratio from 0.039 to 0.022. The main reason for the observed trend could be that the decrease of mean gold particle size causes an initial increase of the Au/C surface atomic ratio. However, at a higher amount of PVA the surface

of gold nanoparticles could be substantially covered by the presence of PVA, causing a decrease in the value of the Au/C surface atomic ratio. In the case of the Au/AC_PVP catalysts, increasing the PVP/Au weight ratio from 0 to 2.4, led to a decrease of the Au/C surface atomic ratio from 0.028 to 0.0013.

Table 2. XPS data for supported Au nanoparticles using PVA and PVP with different polymer to Au weight ratio.

Samples	BE Gold (eV)	Au on Surface (at%)	C on Surface (at%)	N on Surface (at%)	Surface Atomic Ratio Au/C
Au/AC _0	84.0	2.61	91.64	-	0.028
Au/AC_ PVA0.3	84.1	3.48	87.52	-	0.039
Au/AC_ PVA0.6	84.1	2.80	85.80	-	0.033
Au/AC_PVA1.2	84.1	2.40	82.55	-	0.029
Au/AC_PVA2.4	84.1	1.81	82.53	-	0.022
Au/AC_PVP0.3	84.0	1.43	90.94	2.10	0.016
Au/AC_PVP0.65	84.0	1.17	88.69	3.25	0.013
Au/AC_ PVP1.2	84.0	0.15	90.81	2.90	0.0016
Au/AC_PVP2.4	84.1	0.12	89.53	3.60	0.0013

2.2. Catalytic Activity

2.2.1.. Effect of Stabilizer and Polymer to Au Weight Ratio

The catalytic performance of a series of Au/AC_ PVA and Au/AC_PVP supported nanoparticles were investigated for the HDO oxidation to adipic acid by varying the stabilizer to Au weight ratio on the synthesised Au colloidal nanoparticles. In previous studies [21,23], we have shown the importance of tuning the amount of stabilizer for controlling not only the morphological properties of the supported metal nanoparticles but also to influence the activity, the selectivity to desired products and the catalytic stability. A high-pressure batch reactor was firstly used for the initial catalytic screening of the synthesized catalysts at reaction conditions that have been reported in our previous work [41].

Figures 2a,b show the catalytic results obtained for the series of the Au/AC_PVA catalysts as a function of PVA to Au weight ratio and with HDO to Au molar ratio of 50 and 100, respectively. In the case of using HDO/Au molar ratio of 50, the conversion of HDO was in the range of 60–80% and the yield to adipic acid was the highest (40%) when the PVA to Au weight ratio was 1.2. HHA as one of the intermediates was formed with yield of 12–21%. The carbon balance was in the range of 63–82%, suggesting the formation of by-products and adsorption of intermediates and products as has been previously suggested [41]. At HDO/Au molar ratio of 100 (Figure 2b), a lower conversion of HDO was observed, in the range of 23–60%, and the yield to adipic acid decreased from 40% to 6%, whereas the carbon balance was in the range of 70–80%. These results imply that a low HDO to Au molar ratio is necessary to achieve yield to AA around 40%, without the presence of base. However, the high amount of Au catalyst used is not practical and economical for industrial applications. Nevertheless, the experimental conditions that have been chosen are without the use of base, which is well known an essential parameter for activating gold-based catalysts using lower concentration of Au nanoparticles [17,30,42,43]. On the other hand, and in the presence of Au/AC_PVP catalysts, as it is shown in Figures 2c,d, it is evident that the PVP to Au weight ratio has a significant impact in terms of activity and yield to AA. At lower HDO to Au molar ratio of 50, as the PVP to Au weight ratio was increased, a progressive decrease in the conversion of HDO was observed from 60% to 50%, whereas in the case of AA yield a significant decrease from 17% to 8% was observed. The carbon balance was in the range of 80–86% (Figure 2c). At

higher HDO to Au molar ratio of 100, the conversion of HDO was in the range of 25–60%, and the yield to AA, was much lower, (1–3%) and with carbon balance in the range of 73–80% (Figure 2d).

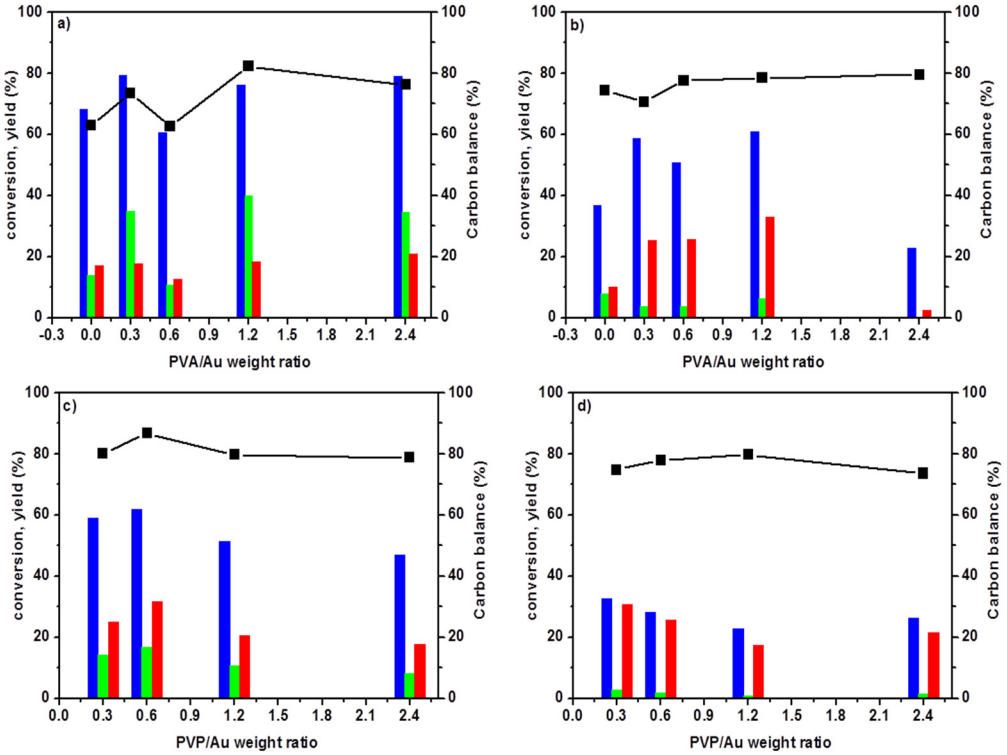

Figure 2. Conversion and yield to products as function of (**a**,**b**) PVA and (**c**,**d**) PVP stabilizer by using (**a**,**c**) nHDO/nAu = 50 and (**b**,**d**) nHDO/nAu = 100: (■) HDO conversion, (■) AA yield, (■) HHA Yield, (■) Carbon balance. Reaction conditions: 2 mL solution of HDO (42 mmol L^{-1}), 110 °C, 15 bar air, 4 h, 600 rpm.

Comparing the two series of Au catalysts, it is evident that in the case of choosing PVP as the desired stabilizer, the conversion of HDO and yield to adipic acid is significantly lower, and especially increasing the PVP to Au weight ratio above 1.2 has a significant impact in terms of activity and yield to AA. Moreover, it is essential to operate at low HDO to Au molar ratio, to activate HDO and produce AA, via the selective oxidation of HHA.

The same series of catalysts were tested under the presence of NaOH (nNaOH/nHDO = 3 molar ratio), with the highest HDO/Au molar ratio of 250 as the positive effect of adding base for the activation of gold catalyst is well known [43,44].

In the case of the Au/AC_PVA catalysts as shown in Figure 3a, the conversion was in the range of 87–95%, and the yield of AA was varied from 3 to 20%. The highest yield to AA was obtained when the PVA/Au weight ratio was 0.6. It is interesting to note that in the presence of NaOH the yield to AA was increased by a factor of 5. The yield of HHA, one of the intermediates was in the range of 76–82%, and the carbon balance was over 88–100% indicating that in the presence of NaOH the rate of transformation of HDO to HHA has been increased, and the formation of by-products and strong adsorption of intermediates/products has been decreased drastically in agreement with the role of base for gold catalysts [43,44].

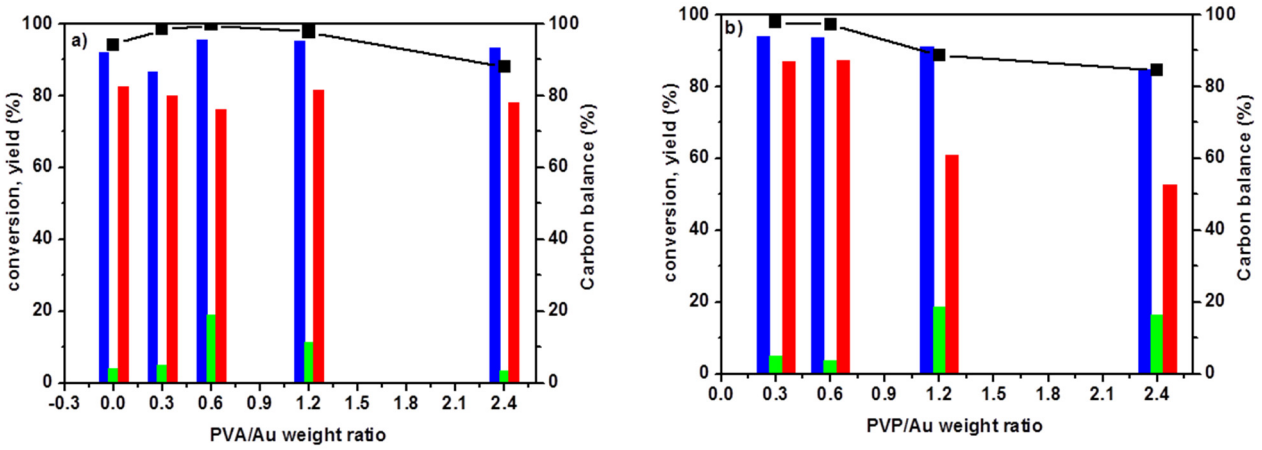

Figure 3. Conversion and yield to products as function of (**a**) PVA and (**b**) PVP stabilizer in the presence of NaOH: (■) HDO conversion, (■) AA yield, (■) HHA Yield, (■) Carbon balance. Reaction conditions: 2 mL solution of HDO (42 mmol L^{-1}), nHDO/nAu =250, 110 °C, 15 bar air, 4 h, 600 rpm, nNaOH/nHDO = 3.

Figure 3b shows the catalytic data for the Au/AC_PVP catalysts in the presence of NaOH. As in the case of the Au/AC_PVA catalysts, an increase of conversion of HDO was observed, as well as in the yield of AA and HHA. Increasing the PVP/Au weight ratio, had a significant impact for the formation of AA, with the maximum value of AA observed with PVP/Au weight ratio of 1.2. It is interesting to note that in the absence of base at high weight ratio of PVP to Au, the yield to AA was below 2%, whereas in the presence of base, AA was formed with yield over 19%. These results imply that the NaOH significantly facilitates the desorption and removal of the PVP stabilizer that creates available free Au active sites, and as a consequence facilitates the activation of HDO but also the transformation of HHA to AA.

2.2.2. Effect of Experimental Conditions on Optimized Au Catalysts

Based on the initial catalytic screening, two catalysts (Au/AC_PVA, Au/AC_PVP) with the polymer/Au weight ratio of 1.2 were chosen for further investigation of different experimental parameters such as the effect of stirring, amount of NaOH, reaction temperature, and reusability.

The effect of stirring rate over the range 800 to 1200 rpm on catalytic conversion of HDO and yield to products was studied under 15 bar of air at 110 °C (Figure 4). In the presence of Au/AC_PVA and Au/AC_PVP catalysts, the yield of AA decreased from 17% and 10% to 4% and 3%, respectively, as the stirring rate increased from 800 to 1200 rpm. This was accompanied with an increase of HHA yield and carbon balance. Finally, over both catalysts, the conversion of HDO was in the range of 97–99%.

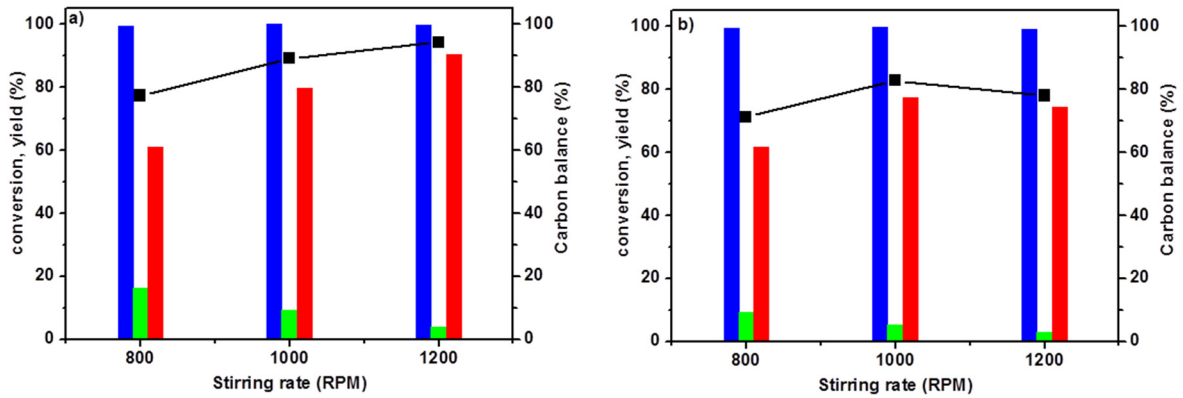

Figure 4. Effect of stirring rate on conversion and yield to products in the presence of (**a**) Au/AC_PVA and (**b**) Au/AC_PVP catalysts: (■) HDO conversion, (■) AA yield, (■) HHA Yield, (■) Carbon balance. Reaction conditions: HDO 42 mmol L^{-1}, 20 mL H_2O, nHDO/nAu =250, 110 °C, 15 bar air, 4 h, stabilizer/Au weight ratio of 1.2.

The effect of NaOH in the range of 1–3 equivalents on catalytic conversion and yield to products was studied in Figure 5. At 110 °C and under 15 bar of air, as the amount of NaOH increased from 1 to 3 equivalents, the conversion increased from 78% to 100% over both catalysts. On the other hand, the yield to AA increased from 1% and 2% to 5.5% and 17%, respectively, in the presence of Au/AC_PVP and Au/AC_PVA catalysts. Moreover, the highest yield to HHA was recorded with three equivalents of NaOH (71% and 75%, respectively). Similar catalytic trends have been observed as in the case of polyol oxidation, especially for the selective oxidation of glycerol to glyceric acid [45,46]. Finally, with all the equivalents of NaOH, the carbon balance was stable over the range of 80% and 90%, respectively, in the presence of Au/AC_PVP and Au/AC_PVA catalysts.

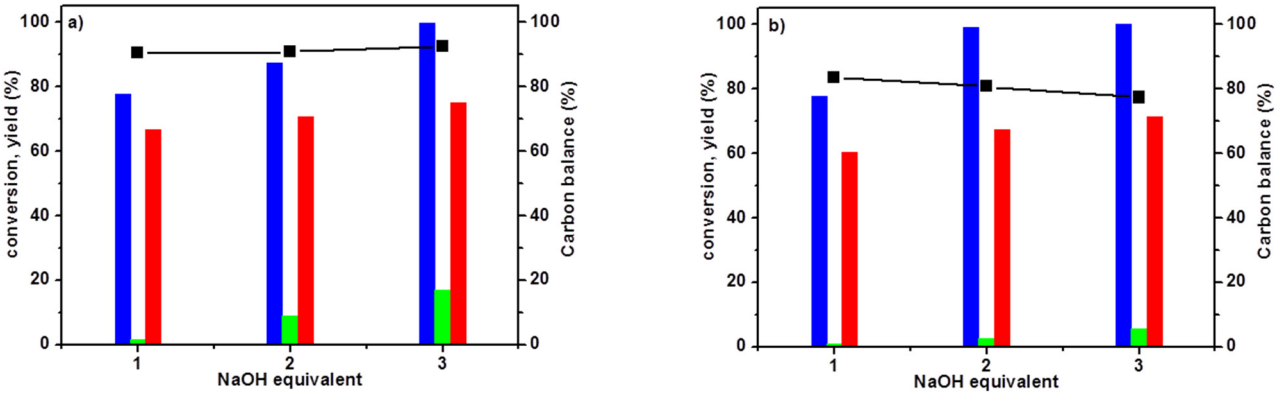

Figure 5. Effect of NaOH amount on conversion and yield to products in the presence of (**a**) Au/AC_PVA and (**b**) Au/AC_PVP catalysts: (■) HDO conversion, (■) AA yield, (■) HHA Yield, (■) Carbon balance. Reaction conditions: HDO 42 mmol L^{-1}, 20 mL H_2O, nHDO/nAu =250, 110 °C, 800 rpm, 15 bar air, 4 h, stabilizer/Au weight ratio of 1.2.

The effect of reaction temperature in the range of 30–140 °C was investigated under 15 bar of air in the presence of Au/AC_PVA and Au/AC_PVP catalysts (Figure 6). Over both catalysts, at lower reaction temperature (30 °C), the main product was HHA with 99% yield and traces of AA was formed. As the temperature increased from 30 to 140 °C, HHA was further oxidized and the yield of AA reached 20% and 30%, respectively, in the presence of Au/AC_PVP and Au/AC_PVA catalysts. However, increasing the reaction

temperature above 110 °C, a significant loss of carbon balance was observed due to following reasons: (i) the increase of formation of side products, such as the formation of gaseous products from the over-oxidation or decarbonylation of aldehydes and acid or di-acid products and (ii) adsorption of intermediates and products on the surface of the catalyst. At higher reaction temperature, it is more reasonable to believe that the promotion of side reactions and over-oxidation is the main reason for the lower carbon balance observed. Therefore, a reaction temperature in the range of 100–110 °C, is beneficial for achieving high conversion, a reasonable yield to AA, and higher carbon balance.

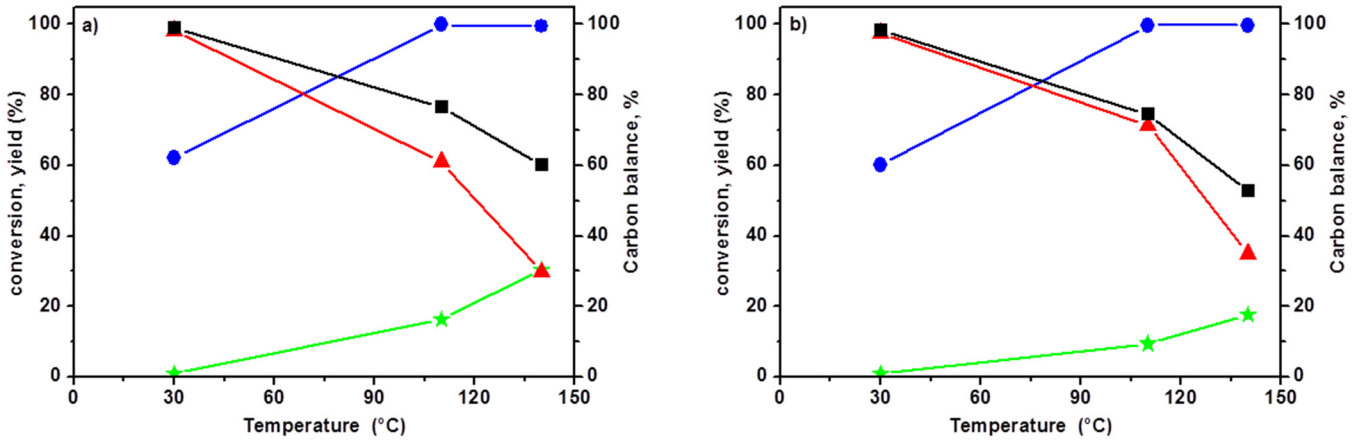

Figure 6. Effect of reaction temperature on conversion and yield to products in the presence of (**a**) Au/AC_PVA and (**b**) Au/AC_PVP catalysts: (●) HDO conversion, (*) AA yield, (▲) HHA Yield, (■) Carbon balance. Reaction conditions: HDO 42 mmol L^{-1}, 20 mL H_2O, nHDO/nAu =250, 800 rpm, 15 bar air, 4 h, stabilizer/Au weight ratio of 1.2.

The effect of HDO/Au molar ratio on catalytic conversion and yield to product is presented in Figure 7. Under 15 bar of air at 110 °C, the conversion level was around 99% over both catalysts. As the HDO/Au molar ratio increased from 250 to 1000, the yield of AA decreased from 16% and 9.4% to 9% and 5%, respectively in the presence of Au/AC_PVP and Au/AC_PVA catalysts. On the other hand, HHA formation was favoured at high HDO/Au molar ratio (~80%). Finally, the carbon balance was increased to attain 85% over both catalysts. These results show that as the number of Au active sites was increased, it promoted the consecutive oxidation of the intermediates, such as HHA to AA. However, at lower HDO/Au molar ratio the formation of side products and adsorption of intermediates/products on the surface of the catalyst is evident.

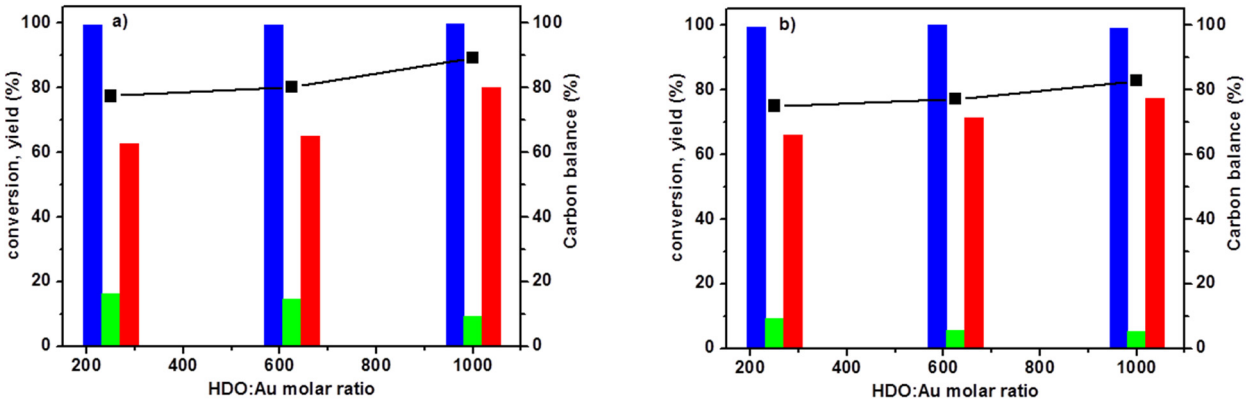

Figure 7. Effect of HDO/Au molar ratio on conversion and yield to products in the presence of (**a**) Au/AC_PVA and (**b**) Au/AC_PVP catalysts: (■) HDO conversion, (■) AA yield, (■) HHA Yield, (■) Carbon balance. Reaction conditions: HDO 42 mmol L^{-1}, 20 mL H_2O, 110 °C, 15 bar air, 800 rpm, 4 h, stabilizer/Au weight ratio of 1.2.

The reusability of the Au/AC_PVA and Au/AC_PVP catalysts was investigated at 110 °C under 15 bar of air. Over both catalysts, the catalytic conversion was constant (~99%) for three runs of reaction (Figure 8). On the other hand, a significant decrease in the formation of AA was observed and after three runs the formation of AA was negligible. Moreover, a decrease of HHA yield and carbon balance was observed after three runs of reactions in the presence of the Au/AC_PVA and Au/AC_PVP catalysts. These results imply that the reasons for the strong deactivation can be due to: (i) a significant restructuring on the surface of the catalyst, (ii) chemical poisoning due to the strong adsorption of intermediates and products on the surface of the catalyst and blocking of the pores of the catalyst, and (iii) Au leaching into the solution.

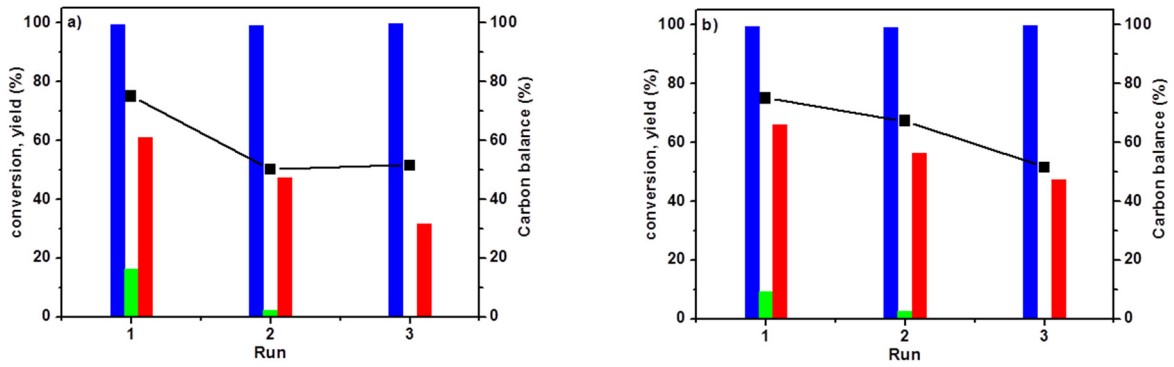

Figure 8. Catalyst recyclability study: (**a**) Au/AC_PVA and (**b**) Au/AC_PVP: (■) HDO conversion, (■) AA yield, (■) HHA Yield, (■) Carbon balance. Reaction conditions: HDO 42 mmol L^{-1}, 20 mL H_2O, nHDO/nAu =250, 110 °C, 800 rpm, 15 bar air, 4 h, stabilizer/Au weight ratio of 1.2.

Nonetheless, no leaching of Au was detected by ICP analysis. XPS and TEM characterizations were performed on the used catalysts to understand the possible reasons for deactivation.

X-ray photoelectron spectroscopy (XPS) was performed on the fresh and spent catalysts. The Au 4f spectra of the Au/AC_PVA and Au/AC_PVP catalysts are displayed in Figure S8. XPS analysis confirmed the metallic state of the Au metal in the fresh and

spent C-supported Au/AC_PVA and Au/AC_PVP materials with BE values of 84.1–84.3 eV for $4f_{7/2}$ component.

The relative abundance of the catalyst components in the fresh and spent C-supported Au-PVA and PVP materials are compiled in Table 3. The presence of Na (1.5%) on the surface of the spent catalysts is due to the use of NaOH. Moreover, it is evident by observing the Au/C surface atomic ratio, a significant decrease was observed that it was higher in the case of the Au/AC_PVP catalyst. Moreover, in the case of the Au/AC-PVP catalyst we observed a reduction of the concentration of the N based on the XPS analysis (Figure S10). The N1s region of the Au/AC_PVP catalyst was analysed and the surface % was slightly lower after catalytic test: 3.17% and 2.42% for fresh and spent sample respectively. These results imply that either can be a significant surface blockage of the active sites from the intermediates and products as well as a surface restructuring of the Au nanoparticles with possible agglomeration and aggregation of the Au nanoparticles and partial removal of the polymer for the surface of the catalyst. To verify this hypothesis, TEM analysis of the spent catalysts was performed (Figure S9). It is evident from TEM analysis that there is a significant increase of mean Au nanoparticle size from 2–7 nm to 14–16 nm and the presence of small medium and large nanoparticles was observed. These results can explain the significant decrease not only of Au/C surface atomic ratio but also in terms of catalytic performance, especially the loss of the formation of AA and the decrease in the formation of HHA.

Table 3. XPS atomic concentration of the components for the fresh and spent Au/AC_PVA and Au/AC_PVP catalysts.

	Atomic Concentration (%)			
Catalysts	**C**	**Au**	**Na**	**Au/C**
Au/AC_PVA Fresh	82.55	2.4	0.0	0.029
Au/AC_PVA Spent	88.32	0.18	1.47	0.002
Au/AC_PVP Fresh	90.81	0.15	0.0	0.0016
Au/AC_PVP Spent	86.22	0.12	1.45	0.001

3. Materials and Methods

3.1. Materials

The supported Au catalysts were prepared by using the sol- immobilization method [31,47–49]. Tetra chloroauric(III) acid (Sigma Aldrich, 99.99 %), poly(vinyl alcohol) (PVA, Sigma Aldrich, MW 13 000–23 000 g mol^{-1}, hydrolysed 87–89 %), poly(vinyl pyrrolidone) (PVP, Sigma Aldrich, MW 29000 g mol^{-1}), poly(ethylene glycol) (PEG, Sigma Aldrich, MW 8000 g mol^{-1}), sulfuric acid (Sigma Aldrich, 98%), sodium borohydride (Sigma Aldrich, powder, ≥98.0%), and activated carbon SX1G (AC, Norit) were used for catalyst preparation and were purchased from Sigma Aldrich (Milan, Italy).

3.2. Catalyst Preparation

A typical preparation protocol is described below: for the preparation of 1 g of catalyst, 0.0209 g of $HAuCl_4 \times 3H_2O$ were dissolved in 390 mL of distilled water (53.58 mg L^{-1} of gold precursor–1.30×10^{-4} M Au). Then, the desired volume of stabilizer (PVA) or (PVP) solution (0.1010 g mL^{-1}) were added as the preferred stabilizing agent for varying the polymer to Au weight ratio from 0 to 1.2. After 3 min, 0.0096 g of sodium borohydride dissolved in 2.5 mL of water was added all at once rapidly to the solution using a calibrated Eppendorf® pipette under stirring ($NaBH_4$: Au = 5:1 molar ratio) to obtain a red colloidal dispersion. The Au colloidal solution was stirred for 30 min (stirring rate of 800 rpm) and 0.99 g of support (activated carbon) was added to the solution to immobilize the gold preformed colloidal nanoparticles. The pH of the solution was adjusted until pH = 2 by the addition of concentrated sulfuric acid. The slurry solution was stirred at room temperature for 1 h (stirring rate of 800 rpm). Then, the catalyst was filtered using a

Buchner funnel. The catalyst was washed several times with distilled water until the filtrated aqueous solution reached pH of 7. Finally, the catalyst was firstly dried overnight at room temperature conditions and afterwards it was dried at 80 °C in an oven for 4 h in static air conditions.

3.3. Characterization of Catalysts

The characterization of the catalysts was performed using UV–vis, XRD, XPS, and TEM techniques. UV–visible spectra of the Au colloidal solutions were recorded on an Agilent Cary 3500 UV–vis spectrometer. XRD analysis of the powder samples was performed with a Bragg–Brentano X'pertPro Panalytical diffractometer using a copper anode (Kα radiation at λ = 1.5418 Å) as the source of X radiation with 0.08° step size and acquisition time of 1300 s per step in 36–41° 2θ range. The calculation of the mean gold crystallite size for the Au/AC catalysts was carried out by using the Scherrer equation: $t = 0.9\lambda/(\beta_{hkl} \times \cos\theta_{hkl})$, where t is the crystallite size, λ is the X-ray wavelength of radiation for Cu Kα, β_{hkl} is the full-width at half maximum (FWHM) at (hkl) peak and θ_{hkl} is the diffraction angle. The Scherrer equation was applied for the Au diffraction peak at 2θ=38.2°, corresponding to the (111) Au plane [50].

Transmission electron microscopy (TEM) images were obtained using a TEM/STEM FEI TECNAI F20 microscope at 200 keV and a TEM Talos F200X instrument. Samples were suspended in ethanol and treated by ultrasound for 15 min. A drop of the suspension was deposited on "quantifoil-carbon film" supported on a Cu grid and dried before analysis. TEM images were processed by using the Digital Micrograph Software by "Gatan Inc." and ImageJ. IA Imaging and Analysis Offline by FEI company for STEM-HAADF images were used in order to determine average particle size and particle size distribution. More than 400 NPs were measured, coming from different sites of interest, for each sample. X-ray photoelectron spectroscopy (XPS) spectra were recorded on a physical electronic spectrometer (PHI Versa Probe II) using monochromatic Al K radiation (52.8 W, 15 kV, 1486.6 eV) and a dual-beam charge neutralizer for analyzing the core-level signals of the elements of interest with a hemispherical multichannel detector. The XPS spectra of the samples were recorded with a constant pass energy value at 29.35 eV and a beam diameter of 100 μm. The energy scale was calibrated using Cu $2p_{3/2}$, Ag $3d_{5/2}$, and Au $4f_{7/2}$ photoelectron lines at 932.7, 368.2, and 83.95 eV, respectively. The X-ray photoelectron spectra obtained were analyzed using PHI SmartSoft software and processed using the MultiPak 9.6.0.15 package. The binding energy values were referenced to C 1 s signal at 284.5 eV. Shirley-type background and Gauss–Lorentz curves were used to determine the binding energies. Atomic concentration percentages of the characteristic elements were determined considering the corresponding area sensitivity factor for the different measured spectral regions.

3.4. Catalytic Test

The catalytic oxidations of HDO were carried out using two catalytic systems: first, the reactions were carried out in a 30 mL TOPIndustry autoclave reactor equipped with a high precision heating system and a mechanical stirrer. In a typical experiment, an aqueous solution (20 mL) of HDO and the appropriate amount of catalyst that corresponds to the HDO/metal molar ratio of 100 were introduced into the reactor. After this, the reactor was closed and purged with a flow of oxygen. The reaction was carried out under 15 bar of air at 110 °C and 600 rpm for 4 h. The time necessary to reach the desired temperature was not considered in the reaction time; indeed the 4 h of reaction started just when the system reached the right temperature. The second system is an Autoplant Workstation from ChemSpeed. Eight fully automated and instrumented high pressure reactors (100 mL) are installed in the workstation. Each reactor is equipped with high-pressure pump, gas flow, and pressure controller. Injection of liquid and/or gas reagent, pressure (up to 80 bar) and temperature (−10 °C to +250 °C) in each reactor can be controlled individually. The reactor heads include an integrated reflux condenser and

houses connectors for temperature and pH probes and liquid sampling. In addition, each reactor includes one feed vessel that is intended for the storage of reagents added to the reactor via the syringe pump in the course of an application. Different stirrer designs (anchor or twisted blade) were used. The reaction was carried out under 15 bar of air at 110 °C for 4 h at different stirring rates. At the end of the reactions, the autoclave was cooled, the pressure was released, and the suspension was collected and filtered with a nylon membrane filter (0.2 μm). AA, HDO, and HA were analysed using a high-performance liquid chromatograph (HPLC, Waters 2410 RJ) equipped with refractive index (RI) and UV detectors and a Rezex ROA-organic acid H+ column (⌀ 7.8 mm × 300 mm). Dilute H_2SO_4 (5 mM, 0.5 mL min^{-1}) was used as a mobile phase. The response factor was determined experimentally for the commercial compounds. It was therefore possible to calculate conversion (X), yield (Y), and carbon balance (CB), according to the following formulas:

$$\text{X HDO (\%)} = \frac{\text{n HDO}_0 - \text{n HDO}_f}{\text{nHDO}_0} \times 100$$

$$\text{Y product (\%)} = \frac{\text{n product}_f}{\text{n HDO}_0} \times 100$$

$$\text{Carbon balance (CB)} = \frac{\text{n HDO}_f + \text{n AA}_f + \text{n HHA}_f}{\text{n HDO}_0} \times 100$$

where $nHDO_0$ is the initial number of moles of HDO, $nHDO_f$ is the final number of moles of HDO, $nproduct_f$ is the final number of moles of products, nAA_f is the final number of moles of adipic acid, and $nHHA_f$ is the final number of moles of HHA.

4. Conclusions

The influence and the amount of stabilizer was investigated in the presence of preformed supported Au colloidal nanoparticles, using activated carbon as the preferred choice of support, for the selective aqueous phase oxidation of 1,6-hexanediol to adipic acid in the absence and presence of base (NaOH). Two specific stabilizers were chosen for the synthesis of preformed Au colloidal nanoparticles: PVA and PVP. The choice and the amount of stabilizer had a significant impact in terms of catalyst activity and formation of AA. When the stabilizer to Au weight ratio was in the range 0.6–1.2 the optimal catalytic performance was obtained in terms of yield to AA. When PVA was the chosen stabilizer, Au/AC_PVA catalysts showed a higher activity and yield of AA, whereas in the case of PVP conversion to HDO and yield to AA was lower. The difference in the catalytic performance was mainly attributed to the stronger interaction and surface coverage of PVP on the active sites of the support and the larger mean Au particle size. Basic conditions significantly improved the yield of AA in both cases. However, in terms of catalyst stability a strong deactivation was observed due to Au nanoparticle agglomeration and weak Au-support interaction when activated carbon was the chosen support. These results demonstrate the strong influence of stabilizer and how important is to tune the stabilizer to weight Au ratio and in the future the nature of support would be investigated for improving not only the catalytic stability but also to facilitate the direction of the reaction pathway to the desired product at relatively mild reaction conditions.

Supplementary Materials: The following are available online at https://www.mdpi.com/2073-4344/8/2/54/s1, Figure S1: UV–vis spectra of Au colloidal solutions with different PVA:Au weight ratio; Figure S2: UV–vis spectra for Au/AC PVP series after 25 min from the addition of $NaBH_4$; Figure S3: XRD patterns of activated carbon and Au/AC samples with different PVA:Au weight ratio; Figure S4: TEM images and particle size distributions of Au/AC synthesized using PVA with different PVA:Au weight ratio; Figure S5: TEM images and particle size distributions of Au/AC

synthesized using PVP with different PVA:Au weight ratio; Figure S6: XPS spectra for Au/AC using PVA with different PVA:Au weight ratio; Figure S7: XPS spectra for Au/AC using PVP with different PVP:Au weight ratio; Figure S8: XPS spectra of the Au4f core levels of the fresh and spent C-supported Au-PVA and Au-PVP catalysts; Figure S9: TEM images and particle size distributions of the spent catalysts (a) Au-PVA/C and (b) Au-PVP/C catalysts; Figure S10: XPS spectra of the N1S core levels of the fresh and spent C-supported Au-PVP catalysts; Table S1: Mean crystallite size for Au/AC using PVA with different PVA:Au weight ratio; Table S2: Mean crystallite size for Au/AC using PVP with different PVP:Au weight ratio.

Author Contributions: Conceptualization, N.D.; Data curation, C.A.G.S., F.M., E.R.-A., J.A.C., A.S., F.O., and R.W.; Formal analysis, E.M., A.V., C.A.G.S., F.M., E.R.-A., J.A.C., A.S., F.O., and R.W.; Investigation, E.M., C.A.G.S., F.M., A.S., and R.W.; Methodology, R.W. and N.D.; Project administration, N.D.; Resources, R.W. and N.D.; Software, F.O.; Supervision, R.W. and N.D.; Writing—original draft, N.D.; Writing—review and editing, E.M., A.V., E.R.-A., J.A.C., F.O., T.T., S.A., F.C., R.W., and N.D. All authors have read and agreed to the published version of the manuscript.

Funding: This research received no external funding.

Institutional Review Board Statement: Not applicable.

Informed Consent Statement: Not applicable.

Data Availability Statement: Data are contained within the article.

Acknowledgments: The REALCAT platform benefits from a state subsidy administrated by the French National Research Agency (ANR) within the frame of the 'Investments for the Future' program (PIA), with the contractual reference 'ANR-11-EQPX-0037'. The European Union, through the FEDER funding administered by the Hauts-de-France Region, has co-financed the platform. Centrale Lille, CNRS, and the University of Lille as well as the Centrale Initiatives Foundation are thanked for their financial contributions to the acquisition and implementation of the equipment of the REALCAT platform. Chevreul Institute (FR 2638), Ministère de l'Enseignement Supérieur, de la Recherche et de l'Innovation, Hauts-de-France Region, and FEDER are acknowledged for supporting and partially funding this work.

Conflicts of Interest: The authors declare no conflict of interest.

References

1. Oppenheim, J.P.; Dickerson, G.L. Adipic acid. In *Kirk-Othmer Encyclopedia of Chemical Technology*, 5th ed.; John Wiley & Sons: Hoboken, NJ, USA, 2004; pp. 553–582.
2. Van de Vyver, S.; Román-Leshkov, Y. Emerging catalytic processes for the production of adipic acid. *Catal. Sci. Technol.* **2013**, *3*, 1465–1479.
3. Beerthuis, R.; Rothenberg, G.; Raveendran Shiju, N. Catalytic routes towards acrylic acid, adipic acid and ε-caprolactam starting from biorenewables. *Green. Chem.* **2015**, *17*, 1341–1361.
4. Rahman, A.; Mupa, M.; Mahamadi, C. A mini review on new emerging trends for the synthesis of adipic acid from metal-nano heterogeneous catalysts. *Catal. Lett.* **2016**, *146*, 788–799.
5. Han, J. A bio-based 'green' process for catalytic adipic acid production from lignocellulosic biomass using cellulose and hemicellulose derived γ-valerolactone. *Energy Convers. Manag.* **2016**, *129*, 75–80.
6. Gunukula, S.; Anex, R.P. Techno-economic analysis of multiple bio-based routes to adipic acid. *Biofuels Bioprod. Bioref.* **2017**, *11*, 897–907.
7. Boussie, T.R.; Dias, E.L.; Fresco, Z.M.; Murphy, V.J. Production of Adipic Acid and Derivatives from Carbohydrate-Containing Materials. U.S. Patent 2010/0317822, 2010.
8. Diamond, G.M.; Murphy, V.; Boussie, T.R. *Modern Applications of High Throughput R & D Heterogenous Catalysis*; Volpe, F., Ed.; Bentham Science Publishers: Al Sharjah, United Arab Emirates, 2014; pp. 288–309.
9. Boussie, T.R.; Dias, E.L.; Fresco, Z.M.; Murphy, V.J.; Shoemaker, J.; Archer, R.; Jiang, H. Production of Adipic Acid and Derivatives from Carbohydrate-Containing Materials. U.S. Patent 2014/8669397, 2014.
10. Wang, T.; Ide, M.S.; Nolan, M.R.; Davis, R.J.; Shanks, B.H. Renewable production of nylon-6,6 monomers from biomass-derived 5-hydroxymethylfurfural (HMF). *Energy Environ. Focus* **2016**, *5*, 13–17.
11. Wan, X.; Zhou, C.; Chen, J.; Deng, W.; Zhang, Q.; Yang, Y.; Wang, Y. Base-free aerobic oxidation of 5-hydroxymethyl-furfural to 2,5-furandicarboxylic acid in water catalyzed by functionalized carbon nanotube-supported Au–Pd alloy nanoparticles. *ACS Catal.* **2014**, *4*, 2175–2185.
12. Lolli, A.; Albonetti, S.; Utili, L.; Amadori, R.; Ospitali, F.; Lucarelli, C.; Cavani, F. Insights into the reaction mechanism for 5-hydroxymethylfurfural oxidation to FDCA on bimetallic Pd–Au nanoparticles. *Appl. Catal. A Gen.* **2015**, *504*, 408–419.

13. Bianchi, C.L.; Canton, P.; Dimitratos, N.; Porta, F.; Prati, L. Selective oxidation of glycerol with oxygen using mono and bimetallic catalysts based on Au, Pd and Pt metals. *Catal. Today* **2005**, *102*, 203–212.
14. Enache, D.I.; Edwards, J.K.; Landon, P., Solsona-Espriu, B.; Carley, A.F.; Herzing, A.A.; Watanabe, M.; Kiely, C.J.; Knight, D.W.; Hutchings, G.J. Solvent-free oxidation of primary alcohols to aldehydes using Au-Pd/TiO_2 catalysts. *Science* **2006**, *311*, 362–365.
15. Villa, A.; Wang, D.; Su, D.; Veith, G.M.; Prati, L. Using supported Aunanoparticles as starting material for preparing uniform Au/Pd bimetallic catalysts. *Phys. Chem. Chem. Phys.* **2010**, *12*, 2183–2189.
16. Hou, W.; Dehm, N.; Scott, R. Alcohol oxidations in aqueous solutions using Au, Pd, and bimetallic AuPd nanoparticle catalysts. *J. Catal.* **2008**, *253*, 22–27.
17. Dimitratos, N.; Lopez-Sanchez, J.A.; Hutchings, G.J. Selective liquid phase oxidation with supported metal nanoparticles. *Chem. Sci*. **2012**, *3*, 20–44.
18. Dias, E.L.; Murphy, V.J.; Shoemaker, J.A.W. Process for Production of Adipic Acid from 1,6-Hexanediol. U.S. Patent 2013/0331606, 2015.
19. Mounguengui-Diallo, M.; Vermersch, F.; Perret, N.; Pinel, C.; Besson, M. Base free oxidation of 1,6-hexanediol to adipic acid over supported noble metal mono- and bimetallic catalysts. *Appl. Catal. A Gen.* **2018**, *551*, 88–97.
20. Mounguengui-Diallo, M.; Sadier, A.; Da Silva Perez, D.; Nikitine, C.; Puchot, L.; Habibi, Y.; Pinel, C.; Perret, N.; Besson, M. Aerobic oxidation of C4–C6 α,ω-diols to the diacids in base-free medium over zirconia-supported (bi)metallic catalysts. *New J. Chem.* **2019**, *43*, 9873–9885.
21. Dimitratos, N.; Villa, A.; Prati, L.; Hammond, C.; Chan-Thaw, C.E.; Cookson, J.; Bishop, P.T. Effect of the preparation method of supported Au nanoparticles in the liquid phase oxidation of glycerol. *Appl. Catal. A Gen.* **2016**, *514*, 267–275.
22. Capelli, S.; Motta, D.; Evangelisti, C.; Dimitratos, N.; Prati, L.; Pirola, C.; Villa, A. Effect of carbon support, capping agent amount, and Pd NPs size for bio-adipic acid production from muconic acid and sodium muconate. *Nanomaterials* **2020**, *10*, 505–522.
23. Freakley, S.J.; Agarwal, N.; McVicker, R.U.; Althahban, S.; Lewis, R.J.; Morgan, D.J.; Dimitratos, N.; Kiely, C.J.; Hutchings, G.J. Gold–palladium colloids as catalysts for hydrogen peroxide synthesis, degradation and methane oxidation: Effect of the PVP stabiliser. *Catal. Sci. Technol.* **2020**, *17*, 5935–5944.
24. Yang, N.; Pattisson, S.; Douthwaite, M.; Zeng, G.; Zhang, H.; Ma, J.; Hutchings, G.J. Influence of stabilizers on the performance of Au/TiO_2 catalysts for CO oxidation. *ACS Catal.* **2021**, *11*, 11607–11615.
25. Li, Y.; El-Sayed, M.A. The effect of stabilizers on the catalytic activity and stability of Pd colloidal nanoparticles in the Suzuki reactions in aqueous solution. *J. Phys. Chem. B* **2001**, *105*, 8938–8943.
26. Ansar, S.M.; Kitchens, C.L. Impact of gold nanoparticle stabilizing ligands on the colloidal catalytic reduction of 4-nitrophenol. *ACS Catal.* **2016**, *6*, 5553–5560.
27. Lee, K.Y.; Lee, Y.W.; Lee, J.H.; Han, S.W. Effect of ligand structure on the catalytic activity of Au nanocrystals. *Colloids Surf. A Physicochem. Eng. Aspects* **2010**, *372*, 146–150.
28. Jia, C.J.; Schüth, F. Colloidal metal nanoparticles as a component of designed catalyst. *Phys. Chem. Chem. Phys*. **2011**, *13*, 2457–2487.
29. Rossi, L.M.; Fiorio, J.L.; Garcia, M.A.S.; Ferraz, C.P. The role and fate of capping ligands in colloidally prepared metal nanoparticle catalysts. *Dalton Trans.* **2018**, *47*, 5889–5915.
30. Campisi, S.; Schiavoni, M.; Chan-Thaw, C.E.; Villa, A. Untangling the role of the capping agent in nanocatalysis: Recent advances and perspectives. *Catalysts* **2016**, *6*, 185–205.
31. Dimitratos, N.; Lopez-Sanchez, J.A.; Morgan, D.; Carley, A.; Prati, L.; Hutchings, G.J. Solvent free liquid phase oxidation of benzyl alcohol using Au supported catalysts prepared using a sol immobilization technique. *Catal. Today* **2007**, *122*, 317–324.
32. Pritchard, J.; Kesavan, L.; Piccinini, M.; He, Q.; Tiruvalam, R.; Dimitratos, N.; Lopez-Sanchez, J.A.; Carley, A.F.; Edwards, J.K.; Kiely, C.J.; et al. Direct synthesis of hydrogen peroxide and benzyl alcohol oxidation using Au−Pd catalysts prepared by sol immobilization. *Langmuir* **2010**, *26*, 16568–16577.
33. Haiss, W.; Thanh, N.T.K.; Aveyard, J.; Fernig, D.G. Determination of size and concentration of gold nanoparticles from UV−Vis spectra. *Anal. Chem.* **2007**, *79*, 4215–4221.
34. Link, S.; El-Sayed, M.A. Size and temperature dependence of the plasmon absorption of colloidal gold nanoparticles. *J. Phys. Chem. B* **1999**, *103*, 4212–4217.
35. Tsunoyama, H.; Sakurai, H.; Ichikuni, N.; Negishi, Y.; Tsukuda, T. Colloidal gold nanoparticles as catalyst for carbon−carbon bond formation: Application to aerobic homocoupling of phenylboronic acid in water. *Langmuir* **2004**, *20*, 11293–11296.
36. Zhong, R.-Y.; Sun, K.-Q.; Hong, Y.-C.; Xu, B-Q. Impacts of organic stabilizers on catalysis of Au nanoparticles from colloidal preparation. *ACS Catal.* **2014**, *4*, 3982–3993.
37. Agarwal, N.; Freakley, S.J.; McVicker, R.U.; Althahban, S.M.; Dimitratos, N.; He, Q.; Morgan, D.J.; Jenkins, R.L.; Willock, D.J.; Taylor, S.H.; et al. Aqueous Au-Pd colloids catalyze selective CH_4 oxidation to CH_3OH with O_2 under mild conditions. *Science* **2017**, *358*, 223–227.
38. Visco, A.M.; Neri, F.; Neri, G.; Donato, A.; Milone, C.; Galvagno, S. X-ray photoelectron spectroscopy of Au/Fe_2O_3 catalyst. *Phys. Chem. Chem. Phys.* **1999**, *1*, 2869–2873.
39. Zwijnenburg, A.; Goosens, A.; Sloof, W.G.; Graje, M.W.J.; Kraan, A.M.; Jongth, L.J.; Makee, M.; Moulijn, J.A. XPS and Mössbauer characterization of Au/TiO_2 propene epoxidation catalysts. *J. Phys. Chem. B* **2002**, *106*, 9853–9862.
40. Dimitratos, N.; Villa, A.; Bianchi, C.L.; Prati, L.; Makkee, M. Gold on titania: Effect of preparation method in the liquid phase oxidation. *Appl. Catal. A* **2006,** *311*, 185–192.

41. Capece, N.; Sadier, A.; Ferraz, C.P.; Thuriot-Roukos, J.; Pietrowski, M.; Zieliński, M.; Paul, S.; Cavani. F.; Wojcieszak, R. Aerobic oxidation of 1,6-hexanediol to adipic acid over Au-based catalysts: The role of basic supports. *Catal. Sci. Technol.* **2020**, *10*, 2644–2651.
42. Hashmi, A.S.K.; Hutchings, G.J. Gold catalysis. *Angewandte Chemie Int. Ed.* **2006**, *45*, 7896–7936.
43. Pina, C.D.; Falletta, E.; Prati, L.; Rossi, M. Selective oxidation using gold. *Chem. Soc. Rev.* **2008**, *37*, 2077–2095.
44. Villa, A.; Dimitratos, N.; Chan-Thaw, C.E.; Hammond, C.; Prati, L.; Hutchings, G.J. Glycerol oxidation using gold-containing catalysts. *Acc. Chem. Res.* **2015**, *48*, 1403–1412.
45. Carrettin, S.; McMorn, P.; Johnston, P.; Griffin, K. Kiely, C.J.; Hutchings, G.J. Oxidation of glycerol using supported Pt, Pd and Au catalysts. *Phys. Chem. Chem. Phys.* **2003**, *5*, 1329–1336.
46. Porta, F.; Prati, L. Selective oxidation of glycerol to sodium glycerate with gold-on-carbon catalyst: An insight into reaction selectivity. *J. Catal.* **2004**, *224*, 397–403.
47. Ferraz, C.; Zielinski, M.; Pietrowski, M.; Heyte, S.; Dumeignil, F.; Rossi, L.M.; Wojcieszak, R. Influence of support basic sites in green oxidation of biobased substrates using Au-promoted catalysts. *ACS Sustain. Chem. Eng.* **2018**, *6*, 16332–16340.
48. Lopez-Sanchez, J.A.; Dimitratos, N.; Hammond, C.; Brett, G.L.; Kesavan, L.; White, S.; Miedziak, P.; Tiruvalam, R.; Jenkins, R.L.; Carley, A.F.; et al. Facile removal of stabilizer-ligands from supported gold nanoparticles. *Nat. Chem.* **2011**, *3*, 551–556.
49. Scurti, S.; Monti, E.; Rodríguez-Aguado, E.; Caretti, D.; Cecilia, J.A.; Dimitratos, N. Effect of polyvinyl alcohol ligands on supported gold nano-catalysts: Morphological and kinetics studies. *Nanomaterials* **2021**, *11*, 879–897.
50. Luciania, S.; Cavani, F.; Dal Santo, V.; Dimitratos, N.; Rossi, M.; Bianchi, C.L. The mechanism of surface doping in vanadyl pyrophosphate, catalyst for n-butane oxidation to maleic anhydride: The role of Au promoter. *Catal. Today* **2011**, *169*, 200–206.